pp. 1–17 (2022)

Personalized computational estimation of relative change in coronary blood flow after percutaneous coronary intervention in short-term and long-term perspectives

S. S. Simakov[*†‡§], T. M. Gamilov[†§¶], A. A. Danilov[*†‡§], F. Liang[¶‖], P. Sh. Chomakhidze[¶], M. K. Gappoeva[‡], A. A. Rebrova[†], and Ph. Yu. Kopylov[¶]

Abstract — Coronary artery disease is the leading cause of mortality worldwide, accounting for 12.8% of all deaths. Although the clinical benefits of treating stenosis with percutaneous coronary intervention (PCI) have been extensively demonstrated, residual myocardial ischemia remains in about 30–50% of patients even after a formally successful PCI. We apply previously developed and validated 1D model of haemodynamics, which distributes terminal hydraulic resistance based on the diameters of the parent vessels and Murray's law by a recursive algorithm. In our new model the terminal resistance is decreased according to a transmural perfusion ratio increase. In contrast to our previous work we calculate the transmural perfusion ratio for personally defined zones. Thus, peripheral hydraulic resistance of myocardial perfusion is personalized based on patient data, which were extracted from computed tomography perfusion images. The model serves as a computational tool for simulating pre- to post-PCI changes in coronary haemodynamics of four patients. We simulate fractional flow reserve (FFR), coronary flow reserve (CFR), instantaneous wave-free ratio (iFR), average flow in selected arteries in hyperemic and rest conditions before PCI and after PCI immediately after the surgery (in a short-term) and in a long-term (several months) perspectives. We conclude that high FFR and iFR values in short-term and long-term perspectives are not necessary correlate with CFR improvement and long-term blood flow recovery in coronary arteries.

Keywords: 1D haemodynamics, coronary circulation, stenosis, myocardial perfusion, boundary conditions, fractional flow reserve, coronary flow reserve, instantaneous wave-free ratio, transmural perfusion ratio

MSC 2010: 65D25, 37M05, 92B99

[*]Marchuk Institute of Numerical Mathematics of the Russian Academy of Sciences, Moscow 119991, Russia

[†]Moscow Institute of Physics and Technology, Dolgoprudny 141701, Russia

[‡]Sechenov University, Moscow 119992, Russia

[§]Sirius University of Science and Technology, Sochi 354340, Russia

[¶]World-Class Research Center 'Digital biodesign and personalized healthcare', I. M. Sechenov First Moscow State Medical University (Sechenov University), Moscow 119992, Russia

[‖]Department of Engineering Mechanics, School of Naval Architecture, Ocean and Civil Engineering, Shanghai Jiao Tong University, 200240 Shanghai, China
E-mail: simakov.ss@phystech.edu

The research was supported by the joint RSF-NSFC project (Russian Science Foundation, grant No. 21-41-00029 and National Natural Science Foundation of China, grant No. 12061131015).

Coronary artery disease (CAD) is the leading cause of mortality worldwide, accounting for 12.8% of all deaths. Coronary computed tomography angiography (CCTA) has become a standard diagnostic technique to evaluate the severity of CAD. Catheter-based fractional flow reserve (FFR) is currently regarded as the reference value for the assessment of haemodynamic severity of CAD [21] and indication for percutaneous coronary intervention (PCI). FFR value is the ratio of pressure after (distal to) stenosis to pressure before the stenosis (or aortic pressure) during the drug-induced hyperemia in the coronary vessels due to their vasodilation. FFR characterizes the maximum possible pressure recovery in large coronary arteries (CAs) after PCI. Values of FFR below 0.8 are considered to be haemodynamically significant and provide recommendations for PCI or other invasive intervention. Coronary flow reserve (CFR) and instantaneous wave-free ratio (iFR) also help to evaluate CAD severity. CFR value is the ratio of coronary blood flow (CBF) during drug-induced hyperemia to CBF in quiet conditions (at rest) [16]. CFR characterizes the maximum possible blood flow recovery in large CAs after PCI. CFR values provide better understanding of CAD severity, but such measurements are rarely performed in common clinical practice due to technical limitations. iFR isolates a specific wave-free period in diastole and uses the ratio of distal coronary pressure to pressure observed in the aorta over the same period [25]. This index is measured in normal conditions without hyperemia and drug administration, however, the measurement requires accurate estimation of the wave-free interval. FFR, CFR, and iFR characterize severity of a lesion in large CAs whose diameter is greater than 0.5 mm.

Although the clinical benefits of treating CAD with PCI have been extensively demonstrated, residual myocardial ischemia (i.e., suboptimal myocardial perfusion) remains in about 30–50% of patients even after a formally successful PCI. Follow-up studies have demonstrated that patients with residual myocardial ischemia have an increased risk of late restenosis and extra revascularization, as well as adverse cardiac events that lead to a high rate of readmission or mortality. In this context, identifying patients with potential post-PCI myocardial ischemia has become the issue of great concern in clinical practice. Studies devoted to mechanisms and determinant factors of post-PCI myocardial ischemia have revealed that existence of residual stenosis or untreated diffuse coronary disease, vulnerable plaque, and coronary microcirculation dysfunction are predictive factors for post-PCI myocardial ischemia. These findings have led to an increasing appeal of combining angiographic examination with myocardial perfusion or myocardial blood flow measurement in the work-up of CAD. Recently, postintervention FFR and/or CFR in CAD evaluation was suggested to improve decision making.

Despite better understanding of post-PCI myocardial ischemia, enhanced strategies for comprehensive evaluation of CAD and advanced techniques for in vivo measurements, several challenging issues hamper patient-specific diagnosis and decision making. A major challenge is the difficulty of quantifying the respective contributions of various potential risk factors to detected post-PCI myocardial ischemia. In clinical settings, assessment of coronary arteries and myocardial per-

fusion are usually image-based, they provide qualitative estimate of the functional status of coronary circulation. To improve risk stratification and implement precise patient-specific therapy, clinicians need to know exact causes of post-PCI myocardial ischemia. Moreover, coronary microcirculation dysfunction detected in over 50% patients suspected of CAD cannot be assessed accurately by analysis of medical images, although it is an important contributor to post–treatment myocardial ischemia and predictor of adverse cardiac events. All these problems largely compromise diagnosis of patients with post-PCI residual myocardial ischemia, leaving a large portion of high-risk patients undertreated.

Myocardial CT perfusion (CTP) provides extensive evaluation of the impairment of myocardial microcirculation and ischemia [24]. CTP diagnostics is performed after administration of iodinated contrast through a catheter by imaging the left ventricular (LV) myocardium during the first pass of the contrast bolus. Iodinated contrast attenuates X-rays proportionally to the iodine content in tissue. Thus myocardial perfusion defects can be directly visualized as hypoattenuating or non-enhancing regions. Hyperemia allows revealing more perfusion abnormalities, and a CTP dataset typically contains rest and stress (hyperemic) conditions.

There are two major correlating sources of CAD: stenosis of CAs and impaired microcirculation of the myocardium [2, 32]. However, this correlation is not explicit [23]: a low FFR value across the stenosis may be a reason for recommendation of PCI which would recover blood flow in large downstream CAs, but the myocardium perfusion still may be low due to an impaired microcirculatory region downstream. This effect may be noticeable in several months after PCI and cause restenosis and recurrent ischemia. PCI procedure is not an optimal decision in this case. A lot of clinical studies investigate perfusion indices [7, 15, 22] or combine FFR with perfusion assessments [5, 17]. Modern mathematical models of coronary circulation rarely incorporate perfusion data for CAD evaluation [13, 19, 27]. A lot of works consider FFR, CFR, or iFR regardless of the state of the microvessels in the myocardium [3, 4, 9].

We propose a novel method to improve patient-specific differentiation and quantification of risk factors to clinically detected post-PCI myocardial ischemia through integrating multi-modality medical images with a computational biomechanical model of the coronary circulation coupled to systemic haemodynamics. To ensure that the method is applicable to conditions of patients before and after PCI, we collected all required clinical data provided by noninvasive CCTA and CTP techniques and recover the structure of large coronary vessels based on the CCTA data. CCTA image quality always limits the number of accessible vessels. Each visible terminal vessel is assumed to supply a separate region of the LV tissue. Our algorithm divides the LV surface in regions associated with vicinities of terminal points of identified CAs. Peripheral hydraulic resistance of myocardial perfusion is personalized based on patient's CTP data and CCTA-specific decomposition of LV.

We apply previously developed and validated 1D model of haemodynamics [11] and distribute terminal hydraulic resistance based on the diameters of the parent coronary vessels and Murray's law by a recursive algorithm. In our model, the

terminal resistance is decreased according to a transmural perfusion ratio (TPR) increase. In contrast to our previous work [27], we calculate TPR for personally defined regions avoiding artificial extrusion of invisible vessels from branches of the left coronary artery.

The resulting model serves as a computational tool for estimation of pre- to post-PCI changes in coronary haemodynamics of four patients. We simulate functional indices (FFR, CFR, and iFR), average flow in selected arteries in stress (hyperemic) and normal (rest) conditions before PCI and after PCI immediately after the surgery (in a short-term) and in a long-term (several months) perspective. We conclude, that high FFR and iFR values in short-term and long-term perspectives do not necessarily correlate with CFR improvement and long-term blood flow recovery in coronary arteries.

The rest of the paper is organized as follows. In Section 1.1 we briefly present the 1D model of coronary circulation. In Section 1.2 we describe in more detail our algorithm for connection of terminal vessels in the 1D model and LV segments and outflow boundary conditions based on CTP data. In Section 1.3 we present data of four anonymous patients. The results of the simulations are given in Section 2. Section 3 contains a discussion, conclusions and future perspectives. Abbreviations used in the text are summarized in Table 2.

1. Methods

1.1. Coronary circulation model

The vascular network of the model consists of a synthetic aortic root and aorta, patient-specific left and right coronary arteries (LCA and RCA) and their branches. The aortic root and the aorta produce physiological boundary conditions. All arterial segments are modelled as straight elastic tubes. The length and diameter of each tube are derived from CT image segmentation [8, 30].

Blood flow in the coronary vascular network and the aorta is simulated by a 1D model of the unsteady axisymmetric flow of Newtonian viscous incompressible fluid through the network of elastic tubes. The 1D haemodynamic model is derived from Navier–Stokes equations. For details we refer to [26, 31]. The model is described briefly as follows. The flow in each vessel satisfies the mass and momentum balances. In arteries the model can be written in the form of nonlinear hyperbolic equations [26]:

$$\frac{\partial \mathbf{V}}{\partial t} + \frac{\partial \mathbf{F}(\mathbf{V})}{\partial x} = \mathbf{G}(\mathbf{V}) \tag{1.1}$$

$$\mathbf{V} = \begin{pmatrix} A \\ u \end{pmatrix}, \qquad \mathbf{F}(\mathbf{V}) = \begin{pmatrix} Au \\ u^2/2 + p(A)/\rho \end{pmatrix}, \qquad \mathbf{G}(\mathbf{V}) = \begin{pmatrix} 0 \\ -8\pi\mu \dfrac{u}{A} \end{pmatrix}$$

where t is the time, x is the distance along the vessel counted from a junction point of vessels, $\rho = 1.060\,\mathrm{kg/m^3}$ is the blood density, $A(t,x)$ is the vessel cross-section area, p is the blood pressure, $u(t,x)$ is the linear velocity averaged over the cross-section,

$\mu = 2.5$ mPa·s is the dynamic viscosity of the blood. The relationship between pressure and cross-section is defined by the wall-state equation

$$p(A) = \rho_w c^2 \left(\exp\left(\frac{A}{\widetilde{A}} - 1 \right) - 1 \right) \tag{1.2}$$

where ρ_w is the vessel wall density (constant), c is the pulse wave velocity, $\widetilde{A}$ is the cross-sectional area of the relaxed vessel. More details on vascular elasticity in 1D models can be found in [29]. At the vascular connections we impose the mass conservation condition and the total pressure continuity

$$\sum_{k=k_1,k_2,\ldots,k_M} \varepsilon_k A_k\left(t,\widetilde{x}_k\right) u_k\left(t,\widetilde{x}_k\right) = 0 \tag{1.3}$$

$$p_k\left(A_k\left(t,\widetilde{x}_k\right)\right) + \frac{\rho u^2\left(t,\widetilde{x}_k\right)}{2} = p_{k+1}\left(A_{k+1}\left(t,\widetilde{x}_{k+1}\right)\right) + \frac{\rho u^2\left(t,\widetilde{x}_{k+1}\right)}{2} \tag{1.4}$$

$$k = k_1, k_2, \ldots, k_{M-1}$$

where k is the index of the vessel, M is the number of the connected vessels, $\{k_1,\ldots,k_M\}$ is the range of the indices of the connected vessels, $\varepsilon = 1, \widetilde{x}_k = L_k$ for incoming vessels, $\varepsilon = -1, \widetilde{x}_k = 0$ for outgoing vessels.

A time-dependent heart outflow function and terminal resistance functions of the coronary network adopt the general haemodynamic model to the coronary circulation [10–12, 14, 28]. The boundary conditions at the aortic root include the blood flow from the heart $Q_H(t,\tau)$:

$$u(t,0)A(t,0) = Q_H(t) \tag{1.5}$$

$$Q_H(t) = \begin{cases} SV \dfrac{\pi}{2\tau} \sin\left(\dfrac{\pi t}{\tau}\right), & 0 \leqslant t \leqslant \tau \\ 0, & \tau < t \leqslant T \end{cases} \tag{1.6}$$

where SV is the stroke volume of the left ventricle, T is the period of the cardiac cycle, τ is the duration of the systole. Inflow parameters SV, T, and τ are extracted from patient data. Section 1.2 presents details on defining terminal resistance at the outflow of peripheral arterial segments.

In our work a stenosis is simulated as a separate vessel with a decreased diameter corresponding to patient data and doubled pulse wave velocity c (1.2). Reduction of the terminal resistance by 70% [3, 19] in (1.10) mimics hyperemia conditions as this provides two- or three-fold increase of the coronary blood flow observed in patients during hyperemia.

We calculate FFR as the ratio of the mean pressure in a coronary artery distal to a stenosis $\overline{P}^h_{\text{dist}}$ to the mean aortic pressure $\overline{P}^h_{\text{aortic}}$ during hyperemia [21]:

$$\text{FFR} = \frac{\overline{P}^h_{\text{dist}}}{\overline{P}^h_{\text{aortic}}}. \tag{1.7}$$

FFR values below 0.8 are generally considered as indications for PCI.

CFR is calculated as the ratio of the mean blood flow through a stenosed vessel during hyperemia $\overline{Q}_{\text{hyp}}$ to the mean blood flow through the stenosed vessel under normal (rest) conditions $\overline{Q}_{\text{rest}}$ [16]:

$$\text{CFR} = \frac{\overline{Q}_{\text{hyp}}}{\overline{Q}_{\text{rest}}}. \tag{1.8}$$

Pathological values of CFR are below 2.0.

iFR is the ratio between the mean pressure in a coronary artery distal to a stenosis $\overline{P}^{w}_{\text{dist}}$ and the mean aortic blood pressure $\overline{P}^{w}_{\text{aortic}}$ during the diastolic wave-free period (WFP) in non-hyperemic conditions [20]:

$$\text{iFR} = \frac{\overline{P}^{w}_{\text{dist}}}{\overline{P}^{w}_{\text{aortic}}}. \tag{1.9}$$

Following [25] we assume that WFP begins after a quarter of diastole and ends 5 ms before the end of diastole. iFR values below 0.9 correspond to haemodynamically significant stenoses.

1.2. CTP-based outflow boundary conditions

We perform a two-stage procedure to specify terminal resistances using patient-specific CTP data.

At the first stage of the algorithm we state outflow boundary conditions assuming that a terminal artery with index k is connected to a venous pressure reservoir with pressure $p_{\text{veins}} = 8$ mmHg by a hydraulic resistance R_k. It is described by Poiseuille pressure drop condition

$$p_k(t, L_k) - p_{\text{veins}} = R_k A_k(t, L_k)\, u_k(t, L_k). \tag{1.10}$$

Compression of terminal coronary arteries by myocardium during systole is an important feature of coronary haemodynamics. To account for the compression, we set $R_k = R_k(t)$ in terminal coronary arteries [3, 10, 11, 27]

$$R_k(t) = \begin{cases} \widehat{R}_k \left(1 + 2\sin\left(\dfrac{\pi t}{\tau}\right)\right), & 0 \leqslant t \leqslant \tau \\ \widehat{R}_k, & \tau < t \leqslant T \end{cases} \tag{1.11}$$

where $\widehat{R}_k$ is the terminal resistance during diastole. According to clinical observations and numerical evidence [3, 9], the base hyperemic diastolic value of the peripheral resistance is set to $R_k^{\text{hyp}} = 0.3\widehat{R}_k$.

The values of $\widehat{R}_k$ are set by the following algorithm. We assume, that the total arterio-venous resistance R_{total} of the systemic circulation produces the pressure

drop $\Delta P = P_{\text{mean}} - p_{\text{veins}}$, where P_{mean} is the mean blood pressure in the brachial artery of the patient. Therefore,

$$R_{\text{total}} = \frac{\Delta P}{Q_{\text{CO}}} \tag{1.12}$$

where Q_{CO} is the average cardiac output (CO)

$$Q_{\text{CO}} = \frac{SV}{T}. \tag{1.13}$$

Arterio-venous resistance R_{total} is split between the terminal resistance of the aorta $R_a = 0.05R_{\text{total}}$ and the total terminal resistance of CAs $R_{\text{cor}} = 0.95R_{\text{total}}$. These values provide the ratio of CBF to CO about 3–6%. The total hydraulic resistance of the coronary network R_{cor} is distributed among terminal CAs by a recursive algorithm [27] using diameters of CAs and Murray's law with power 2.27. The resulting base values of terminal resistances $\widehat{R}_k$ are prescribed to each terminal branch.

At the second stage of the algorithm we adopt the peripheral resistance using the patient-specific CTP data which characterize the myocardium perfusion. CTP images present the brightness of the iodinated contrast agent administrated to the arterial blood and transferred through the microcirculation. The brightness of the contrast is proportional to the volumetric blood flow and the oxygen delivery to myocardium. Brighter regions correspond to a higher concentration of the contrast, and faint regions correspond to a lower concentration of the contrast.

CTP workstation automatically divides a geometric model of myocardium into three layers: subendocardium, midwall, and subepicardium. Each layer is divided into sixteen standard zones (regions). The straightforward approach of mapping between terminal coronary vessels and standard regions can not be automatized. Moreover, the number of segmented vessels depends on the quality of CCTA data and differs from patient to patient and from time to time even for particular patient. We overcome this issue by a new algorithm which generates segmentation-specific regions. Each region is identified by geometric proximity to one of the terminal points of the segmented vessels using the Euclidean norm. Our algorithm calculates the mean attenuation density (AD) of each myocardial layer in every segmentation-specific region using detailed CTP data. AD characterizes the impairment of the perfusion in a particular region by the transmural perfusion ratio (TPR)

$$\text{TPR} = \frac{AD_{\text{end}}}{AD_{\text{ep}}} \tag{1.14}$$

where AD_{end} is subendocardial AD and AD_{ep} is subepicardial AD. Two available datasets present TPR measurements at rest and stress states. The rest state corresponds to quiet patient conditions. The stress state is a state with increased blood due to administration of a vasodilating drug (adenosine) which increases lumens of vessels and decreases the hydraulic resistance.

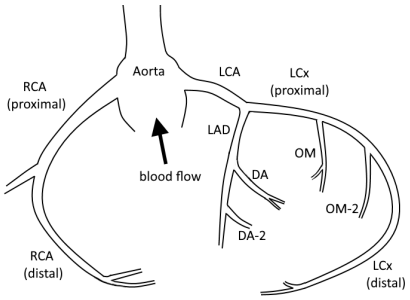

Figure 1. Major coronary arteries and their branches.

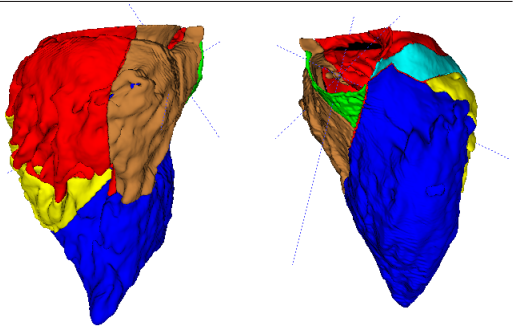

Figure 2. Patient-specific decomposition of the left ventricle: two opposite views.

Table 1. Parameters of the patients: P_{sys} is the systolic pressure, P_{diast} is the diastolic pressure, HR is the heart rate, SV is the stroke volume, R_{tot} is the total hydraulic resistance of the coronary arteries.

No	Age	P_{sys}, mm Hg	P_{diast}, mm Hg	HR, bpm	SV, ml	R_{tot}, mm Hg · s/ml
1	70	140	80	84	65	0.97
2	70	135	80	89	33	1.79
3	68	120	70	62	53	1.35
4	56	107	76	64	35	1.98

Table 2. Abbreviations.

AD	Mean attenuation density	FFR	Fractional flow reserve
CA	Coronary arteries	HR	Heart rate
CAD	Coronary artery disease	iFR	Instantaneous wave-free ratio
CBF	Coronary blood flow	LV	Left ventricle
CFR	Coronary flow reserve	LAD	Left anterior descending artery
CO	Cardiac output	LCA	Left coronary artery
CT	Computed tomography	LCx	Circumflex artery
CTP	Computed tomography perfusion	OM	Obtuse marginal artery
CCTA	Coronary computed tomography angiography	PCI	Percutaneous coronary intervention
		RCA	Right coronary artery
DA	Diagonal branch of LAD	SV	Stroke volume
DAd	Distal part of DA	TPR	Transmural perfusion ratio
DAp	Proximal part of DA		

Finally, we update the base values of the terminal resistances $\widehat{R}_k$ with respect to measured TPR values. TPR values range from 0.0 to 2.0. Values above 1.0 are considered to be healthy. In clinical practice all TPR values above 1.0 are often represented as 1.0 since there is no difference between 1.0 and 2.0 from diagnostic point of view. Assuming that lower TPR values correspond to impaired perfusion and greater hydraulic resistance of the perfusion region, we multiply each base resistance R_k by a coefficient

$$\alpha_k = \begin{cases} 1, & \text{TPR}_k \geqslant 1.0 \\ \exp\left(a(1-\text{TPR}_k)\right), & \text{TPR}_k < 1.0 \end{cases} \tag{1.15}$$

where TPR_k is the TPR value of corresponding LV region. We set $a = 11.6$ so that

$\alpha = 2$ for TPR $= 0.94$. TPR $= 0.94$ is a threshold value for a severe perfusion disorder. Correction (1.15) of outflow boundary condition (1.10) increases the peripheral resistance in regions with low TPR mimicking microcirculation pathology. For those myocardium regions where TPR is not measured, we set the peripheral resistance intact, $\alpha_k = 1$.

1.3. Patient data

This study involves anonymous data from four patients with ischemic heart disease. The patients underwent the contrast-enhanced coronary CT at rest and the adenosine-enabled stress CT perfusion for the left ventricle (CTP). A summary of data from the patient's records is shown in Table 1.

The general anatomical structure of major coronary arteries is shown in Fig. 1 (see Table 2 for abbreviations). The CT data are processed by a segmentation algorithm [8, 30, 31] which produces four patient-specific coronary networks for each patient: in rest or stress conditions and before/after the PCI or a few months later. The results of segmentation for patient 1 are presented in the left parts of Figs. 3–6. Associated geometric parameters of the arterial networks are presented in Tables 7–10. The aortic root is simulated as a vessel with the length 5 cm and diameter 2.3 cm. The aorta is represented by a vessel with the length 80 cm and diameter 2.17 cm. The coronary perfusion is given by CTP images.

The new algorithm for patient-specific decomposition of myocardium inputs the segmented terminal coronary arteries and their position in space. An example of decomposition is shown in Fig. 2. Bull's eye maps of the patient 1 LV decompositions associated with four CCTA (rest or stress, before/after PCI or long term) are shown in the right parts of Figs. 3–6. Figures 3 and 4 present data before or immediately after PCI at rest and stress conditions. Figures 5 and 6 present data several months later at rest and stress conditions. TPR is evaluated by regional averaging voxel data from CTP. Anonymized data of the other three patients are available upon a request.

Patient 1 has occlusions in RCA and LCx (stenosis more than 95%) and 60–75% stenosis in LAD. Patient 2 has occlusion in RCA, 50–60% stenosis in the proximal and middle parts of LAD and 60–75% stenosis in DA. Patient 3 has 75% stenosis in the proximal part of LCx and another 50-75% stenosis downstream in OM branch and a minor 50% stenosis in RCA. Patient 4 has 75–80% stenosis in the middle part of RCA and 60% in the second OM branch of LCx.

For patient 1 stents were installed in RCA and LCx, the second CTP was performed after six months. For patient 2 a stent was installed in RCA, the second CTP was performed after five months. For patient 3 a stent was installed in the proximal part of LCx, the second CTP was performed after four months. For patient 4 a stent was installed in RCA, the second CTP was performed after one month.

Table 3. Simulated parameters of patient 1.

Artery	Period	FFR	iFR	CFR	Q_{rest}, ml	Q_{hyp}, ml
RCA	Before PCI	0.12	0.23	1.70	0.03	0.06
	After PCI	0.99	1.00	2.8	1.07	3.00
	Long-term	0.98	0.99	2.69	1.4	3.76
LCx	Before PCI	0.11	0.38	1.82	0.03	0.05
	After PCI	0.99	0.99	3.70	0.33	1.22
	Long-term	0.99	0.99	2.36	0.39	0.91
LAD	Before PCI	0.76	0.95	1.72	0.08	0.14
	After PCI	0.76	0.96	2.10	0.06	0.13
	Long-term	0.65	0.98	70	0.01	0.7

Table 4. Simulated parameters of patient 2.

Artery	Period	FFR	iFR	CFR	Q_{rest}, ml	Q_{hyp}, ml
RCA	Before PCI	0.4	0.6	1.25	0.01	0.01
	After PCI	0.98	0.99	3.00	0.65	1.96
	Long-term	0.98	0.99	2.95	0.66	1.95
LAD	Before PCI	0.77	0.86	2.14	0.54	1.15
	After PCI	0.87	0.95	2.74	0.25	0.69
	Long-term	0.87	0.89	2.66	0.19	0.49
DA	Before PCI	0.69	0.89	2.30	0.01	0.02
	After PCI	0.83	0.96	2.95	0.004	0.013
	Long-term	0.86	0.93	3.31	0.001	0.003

Table 5. Simulated parameters of patient 3.

Artery	Period	FFR	iFR	CFR	Q_{rest}, ml	Q_{hyp}, ml
RCA	Before PCI	0.96	0.96	2.54	0.78	1.99
	After PCI	0.96	0.96	2.6	0.78	2.03
	Long-term	0.95	0.96	1.98	0.31	0.61
LCx	Before PCI	0.93	0.74	0.13	0.42	0.06
	After PCI	0.93	0.99	2.33	0.55	1.27
	Long-term	0.97	0.98	2.81	0.61	1.71
OM	Before PCI	0.76	0.74	0.57	0.1	0.06
	After PCI	0.79	0.94	9.84	0.13	1.27
	Long-term	0.88	0.95	2.74	0.18	0.48

Table 6. Simulated parameters of patient 4.

Artery	Period	FFR	iFR	CFR	Q_{rest}, ml	Q_{hyp}, ml
RCA	Before PCI	0.71	0.75	2.09	0.52	1.09
	After PCI	0.98	0.99	2.92	0.59	1.72
	Long-term	0.97	0.99	3.16	0.58	1.83
OM	Before PCI	0.91	0.96	1.98	0.17	0.33
	After PCI	0.91	0.96	1.96	0.17	0.32
	Long-term	0.96	0.99	3.34	0.04	0.12

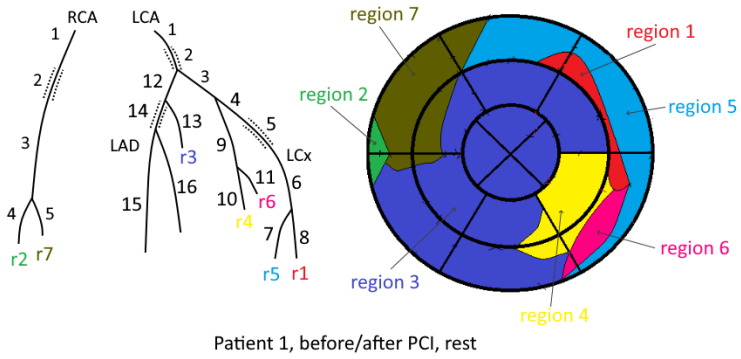

Figure 3. Segmented coronary tree (left) and regional decomposition (right) for patient 1 at rest before and immediately after PCI. Dotted lines designate stenoses. Terminal segments without corresponding region are considered to supply other heart chambers (left atrium, right ventricle). Parameters of segmented tree are presented in Table 7.

Table 7. Patient 1 segmented coronary tree parameters at rest before and immediately after PCI; k is the segment index, l_k is the segment length, d_k is the segment diameter, TPR_k is the TPR value used for terminal resistance calculation (1.15).

LCA	k	1	2	3	4	5	6	7	8	9	10	11	12	13	14	15	16
	l_k, mm	3.6	6.9	11	14	3.5	58	13.5	21.5	32	31.5	5.9	11.4	17.5	10	13	44
	d_k, mm	3	2.2	2.9	3.1	0.2	3.2	1.9	1.7	2.2	2	1.4	2.9	1.5	0.8	2	2
	TPR_k							0.99	0.97		0.90	0.97		0.97		1.0	1.0
RCA	k	1	2	3	4	5											
	l_k, mm	27	3.7	98	8.9	13.3											
	d_k, mm	3.9	0.2	2.9	1.4	1.4											
	TPR_k				0.97	0.97											

2. Results

We used the patient data (see Section 1.3) and the patient-specific mathematical model (see Sections 1.1, 1.2) to study the change of haemodynamic indices FFR, iFR, CFR and the mean flows in the stenosis locations or downstream. The models were validated using the available patient data. The following simulated and measured values coincide with high accuracy (less than 1%): FFR in LAD and DA of patient 2 before PCI, iFR in DA of patient 3 before PCI; FFR in RCA and OM of patient 4 before PCI as well as FFR of patient 4 in RCA immediately after PCI. The other values of haemodynamic indices were unavailable.

We simulate coronary haemodynamics at three successive states: before PCI, immediately after PCI, and in a several months later. Results of the simulation are presented in Tables 3–6. Notations of the coronary arteries can be found in Table 2 and in Figs. 3–6.

We observe stable increase of FFR and iFR in most patients in both short-term and long-term perspectives for both stented and untreated stenoses. In contrast,

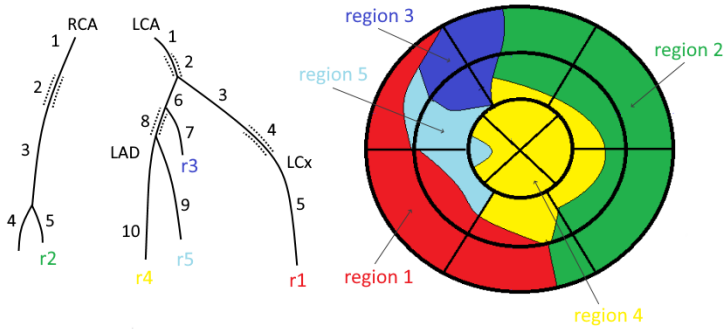

Figure 4. Segmented coronary tree (left) and regional decomposition (right) for patient 1 during stress (hyperemia) before and immediately after PCI. Dotted lines designate stenoses. Terminal segments without corresponding region are considered to supply other heart chambers (left atrium, right ventricle). Parameters of segmented tree are presented in Table 8.

Table 8. Patient 1 segmented coronary tree parameters during stress (hyperemia) before and immediately after PCI. k is the segment index, l_k is the segment length, d_k is the segment diameter, TPR_k is the TPR value used for terminal resistance calculation (1.15).

LCA	k	1	2	3	4	5	6	7	8	9	10
	l_k, mm	2.9	7.3	21	3.5	24	24.3	20	10.1	58.8	116
	d_k, mm	2.9	2.2	3.9	0.2	4.2	3.3	2.2	0.9	2.5	2.6
	TPR_k					1.0		0.98		0.96	1.0
RCA	k	1	2	3	4	5					
	l_k, mm	27	3.7	86	2.1	21					
	d_k, mm	3.9	0.2	3.1	1.1	1.6					
	TPR_k				1.0	0.95					

minor or moderate decrease of CFR is observed in most arteries of patients 1, 2, and 3 in the long-term perspective. The computed CFR values in LAD (long-term) of patient 1 and in OM (after PCI) of patient 3 are not feasible since the vascular structure and the CCTA-based parameters deviate substantially in different states.

Technical limitations hamper direct measurements of the flow in arteries, however, the simulations allow us to compare in Tables 3–6 the absolute values of Q_{rest} and Q_{hyp}. In all considered datasets we observe increase of the mean flow in the rest and stress states immediately after PCI. In contrast, the long-term change of the flows does not have a clear tendency: LCx and LAD of patient 1, LAD and DA of patient 2, OM of patient 3, OM of patient 4 demonstrate decrease of Q_{rest} and Q_{hyp}. It is worth mentioning that PCI for patient 2 was performed in RCA which is separate from LCA with its branches, and interconnection of the flows in RCA and LCA via their common parent vessel (aortic root) results in stable decrease of Q_{rest} and Q_{hyp} in DA of patient 2 in short-term and long-term perspectives.

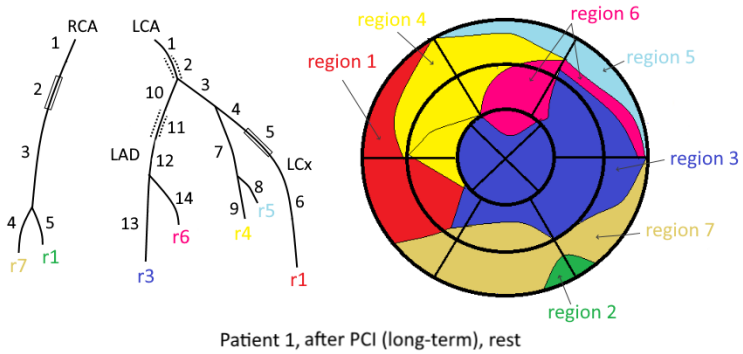

Figure 5. Segmented coronary tree (left) and regional decomposition (right) for patient 1 at rest a few months after PCI. Dotted lines designate stenoses. Rectangles represent stents. Terminal segments without corresponding region are considered to supply other heart chambers (left atrium, right ventricle). Parameters of segmented tree are presented in Table 9.

Table 9. Patient 1 segmented coronary tree parameters at rest a few months after PCI. k is the segment index, l_k is the segment length, d_k is the segment diameter, TPR_k is the TPR value used for terminal resistance calculation (1.15).

LCA	k	1	2	3	4	5	6	7	8	9	10	11	12	13	14
	l_k, mm	3.1	6.8	12.9	5.3	3.2	106	31	2.9	44.7	37	8.7	5	138	45.6
	d_k, mm	3.8	2.9	2.9	4.6	3.9	3.3	2.7	2.3	2.4	2.9	0.8	2.8	2.3	2.7
	TPR_k						0.99		0.99	0.99				0.99	1.0
RCA	k	1	2	3	4	5									
	l_k, mm	42	25	81	6.6	15.5									
	d_k, mm	4.4	3.7	34	2.3	1.8									
	TPR_k				0.99	0.98									

3. Conclusions

We performed computational analysis of coronary blood flow using data of patients underwent the percutaneous coronary intervention (PCI). We aimed to shed the light on possible secondary deprivation after PCI in a long-term perspective. For this purpose we compared simulated haemodynamic parameters before the PCI, immediately after the PCI and in a few months. Our computational model includes the 1D haemodynamic model of coronary circulation in patient-specific geometric domain based on CCTA data. The outflow boundary conditions of this model adopt the CTP data and therefore a possible impairment of myocardial microcirculation. The blood flow in coronary vessels and in microcirculation are combined by a new algorithm, which decomposes the LV surface into regions according to position of terminal vessels available after segmentation of CCTA image. The algorithm provides a one-to-one relationship between terminal vessels and microcirculatory regions. Average TPR values are computed for every region and used in the boundary conditions. On the basis of the new model we computed haemodynamic indices FFR, CFR, iFR

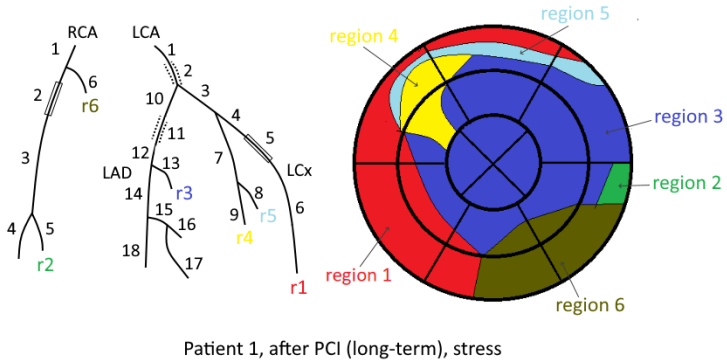

Figure 6. Segmented coronary tree (left) and regional decomposition (right) for patient 1 during stress (hyperemia) a few months after PCI. Dotted lines designate stenoses. Rectangles represent stents. Terminal segments without corresponding region are considered to supply other heart chambers (left atrium, right ventricle). Parameters of segmented tree are presented in Table 10.

Table 10. Patient 1 segmented coronary tree parameters during stress (hyperemia) a few months after PCI. k is the segment index, l_k is the segment length, d_k is the segment diameter, TPR_k is the TPR value used for terminal resistance calculation (1.15).

LCA	k	1	2	3	4	5	6	7	8	9	10	11	12	13	14	15	16	17	18
	l_k, mm	3.0	6.5	12	22	3.3	88	30	88	46	22	12	9	17	12	84	9.3	48	110
	d_k, mm	3.7	2.8	2.9	2.9	3.8	3.2	2.5	1.6	1.8	2.9	0.8	3	1.9	3.7	3.1	1.4	2.2	2.2
	TPR_k						1.0		1.0	1.0				1.0			1.0	1.0	1.0
RCA	k	1	2	3	4	5	6												
	l_k, mm	16	26	101	12	16	3.7												
	d_k, mm	3.7	3.6	3.4	2.1	1.7	1.2												
	TPR_k				1.0	0.99	1.0												

and the mean blood flow in arteries with stenoses or after PCI. These parameters are difficult (or expensive) to measure directly in a patient. Our approach provides the new numerical tool for extensive evaluation and analysis of the coronary blood flow with CAD and after PCI in short-term and long-term perspectives.

Wherever possible we compared computed and measured values and observed discrepancy less than 1%. Clinical studies [1] show that there is a redistribution of regional blood flow from regions supplied by severely stenosed coronary arteries to those supplied by less diseased or normal arteries. In our simulations we also observed this effect, particularly for patient 2. Stenting occlusion in RCA increased blood flow through RCA and decreased blood flow through LAD and DA (branches of LCA) resulting in a significant change of FFR in LAD and DA. We found that high FFR and iFR values in short-term and long-term perspectives do not necessarily correlate with CFR improvement and long-term blood flow recovery in coronary arteries.

We analyzed datasets from four patients; more clinical cases are required for the development and validation of a robust computational tool applicable in clin-

ical practice. In this work, we utilized CTP images for computing TPR values in specific segments to assess myocardial perfusion. The other methods, such as PET (Positron Emission Tomography) perfusion, SPECT (Single Photon Emission Computed Tomography) perfusion, give more accurate 3D distribution of myocardial blood flow and can increase effectiveness of the proposed approach.

Sensitivity of the results to the quality of CT data is the issue to be addressed in future research. We observed substantially different results of segmentation even for the same patient at different times (e.g., before and a few months after PCI). Some arteries may not be visualized and some arteries may vary in size. This led to non-physiological values of long-term CFR in LAD of patient 1 and long-term CFR in OM of patient 3 (see Tables 3, 5). The other issue of CT images is that generated 1D networks contain a small number of terminal vessels. As a result, a relatively small number of the microcirculatory regions affects the specificity of the TPR values and resolution of the regions with impaired microcirculation. Our previous approach [27] operated with sixteen standard regions of LV which give sufficient resolution of impairments at the cost of extrusion of virtual vessels with unknown parameters.

The advantage of the presented approach is availability of TPR perfusion assessment in everyday clinical practice via CTP measurements. The data describing the structure of coronary vessels and the data describing functionality of microcirculation may be acquired within single procedure. This simplifies the examination protocol for both patients and clinicians.

Acknowledgment: The authors acknowledge the staff of Sechenov University especially Nina Gagarina and Ekaterina Fominykh for patient-specific FFR and CTP data.

References

1. R. R. Baliga, S. D. Rosen, P. G. Camici, and J. S. Kooner, Regional myocardial blood flow redistribution as a cause of postprandial angina pectoris. *Circulation* **97** (1998), No. 12, 1144–1149.

2. P. G. Camici and M. Magnoni, How important is microcirculation in clinical practice? *Eur. Heart J. Suppl.* **21** (2019), B25–B27.

3. J. M. Carson, S. Pant , C. Roobottom, R. Alcock, P. J. Blanco, C. A. Carlos Bulant, Y. Vassilevski, S. Simakov, T. Gamilov, R. Pryamonosov, F. Liang, X. Ge, Y. Liu, and P. Nithiarasu, Non-invasive coronary CT angiography-derived fractional flow reserve: A benchmark study comparing the diagnostic performance of four different computational methodologies. *Int. J. Numer. Meth. Biomed. Engrg.* **35** (2019), No. 10, e3235.

4. J. M. Carson, C. Roobottom, R. Alcock, and P. Nithiarasu, Computational instantaneous wave-free ratio (IFR) for patient-specific coronary artery stenoses using 1D network models. *Int. J. Numer. Meth. Biomed. Engrg.* **35** (2019), No. 11, e3255.

5. A. Coenen, A. Rossi, M. M. Lubbers, A. Kurata, A. K. Kono, R. G. Chelu, S. Segreto, M. L. Dijkshoorn, A. Wragg, R.-J. M. van Geuns, F. Pugliese, and K. Nieman, Integrating CT myocardial perfusion and CT-FFR in the work-up of coronary artery disease. *JACC: Cardiovasc. Imaging* **10** (2017), No. 7, 760–770.

6. A. Coenen, M. M. Lubbers, A. Kurata, A. Kono, A. Dedic, R. G. Chelu, M. L. Dijkshoorn, A. Rossi, R. M. van Geuns, and K. Nieman, Diagnostic value of transmural perfusion ratio derived from dynamic CT-based myocardial perfusion imaging for the detection of haemodynamically relevant coronary artery stenosis. *Eur. Radiol.* **27** (2017), No. 6, 2309–2316.

7. R. C. Cury, T. A. Magalhes, A. T. Paladino, A. A. Shiozaki, M. Perini, T. Senra, P. A. Lemos, R. C. Cury, and C. E. Rochitte, Dipyridamole stress and rest transmural myocardial perfusion ratio evaluation by 64 detector-row computed tomography. *J. Cardiovasc. Comput. Tomography* **5** (2011), No. 6, 443–448.

8. A. Danilov, Yu. Ivanov, R. Pryamonosov, and Yu. Vassilevski, Methods of graph network reconstruction in personalized medicine. *Int. J. Numer. Meth. Biomed. Engrg.* **32** (2016), No. 8, e02754.

9. T. M. Gamilov, P. Yu. Kopylov, R. A. Pryamonosov, and S. S. Simakov, Virtual fractional flow reserve assessment in patient-specific coronary networks by 1D haemodynamic model. *Russ. J. Numer. Anal. Math. Modelling* **30** (2015), No. 5, 269–276.

10. T. M. Gamilov, F. Y. Liang, and S. S. Simakov, Mathematical modeling of the coronary circulation during cardiac pacing and tachycardia. *Lobachevskii J. Math.* **40** (2019), No. 4, 448–458.

11. T. Gamilov, P. Kopylov, M. Serova, R. Syunyaev, A. Pikunov, S. Belova, F. Liang, J. Alastruey, and S. Simakov, Computational analysis of coronary blood flow: The role of asynchronous pacing and arrhythmias. *Mathematics* **8** (2020), No. 8, 1205.

12. T. Gamilov and S. Simakov, Blood flow under mechanical stimulations. *Advances in Intelligent Systems and Computing* (2020), *1028 AISC*, 143–150.

13. X. Ge, Y. Liu, S. Tu, S. Simakov, Y. Vassilevski, and F. Liang, Model-based analysis of the sensitivities and diagnostic implications of FFR and CFR under various pathological conditions. *Int. J. Numer. Meth. Biomed. Engrg.* **35** (2019), e3257.

14. X. Ge, S. Simakov, Y. Liu, and F. Liang, Impact of arrhythmia on myocardial perfusion: A computational model-based study. *Mathematics* **9** (2021), No. 17, 2128.

15. R. T. George, A. Arbab-Zadeh, J. M. Miller, K. Kitagawa, H. J. Chang, D. A. Bluemke, L. Becker, O. Yousuf, J. Texter, A. C. Lardo, and J. A. Lima, Adenosine stress 64- and 256-row detector computed tomography angiography and perfusion imaging: a pilot study evaluating the transmural extent of perfusion abnormalities to predict atherosclerosis causing myocardial ischemia. *Circulation. Cardiovascular Imaging* **2** (2009), No. 3, 174–182.

16. K. L. Gould, R. L. Kirkeeide, and M. Buchi, Coronary flow reserve as a physiologic measure of stenosis severity. *J. Amer. Coll. Cardiol.* **15** (1990), No. 2, 459–474.

17. A. R. Ihdayhid, T. Sakaguchi, J. J. Linde, M. H. Srgaard, K. F. Kofoed, Y. Fujisawa, J. Hislop-Jambrich, N. Nerlekar, J. D. Cameron, R. K. Munnur, M. Crosset, D. Wong, S. K. Seneviratne, and B. S. Ko, Performance of computed tomography-derived fractional flow reserve using reduced-order modelling and static computed tomography stress myocardial perfusion imaging for detection of haemodynamically significant coronary stenosis. *Eur. Heart J. Cardiovasc. Imaging* **19** (2018), No. 11, 1234–1243.

18. A. Jeremias, A. J. Kirtane, and G. W. Stone, A test in context: Fractional flow reserve: accuracy, prognostic implications, and limitations. *J. Amer. Coll. Cardiol.* **69** (2017), No. 22, 2748–2758.

19. E. W. Lo, L. J. Menezes, and R. Torii, On outflow boundary conditions for CT-based computation of FFR: Examination using PET images. *Medical Engrg. & Phys.* **76** (2020), 79–87.

20. S. S. Nijjer, S. Sen, R. Petraco, R. Sachdeva, F. Cuculi, J. Escaned, C. Broyd, N. Foin, N. Hadjiloizou, R. A. Foale, I. Malik, G. W. Mikhail, A. S. Sethi, M. Al-Bustami, R. R. Kaprielian, M. A. Khan, C. S. Baker, M. F. Bellamy, A. D. Hughes, J. Mayet, R. K. Kharbanda, C. Di Mario, and J. E. Davies, Improvement in coronary haemodynamics after percutaneous coronary intervention: assessment using instantaneous wave-free ratio. *Heart* **99** (2013), No. 23, 1740–1748.

21. N. H. J. Pijls, B. de Bruyne, K. Peels, P. H. van der Voort, H. J..R..M. Bonnier, J. Bartunek, and J. J. Koolen, Measurement of fractional flow reserve to assess the functional severity of coronary-artery stenoses. *New England J. Medicine* **334** (1996), No. 26, 1703–1708.

22. A. Ruiz-Muoz, F. Valente, L. Dux-Santoy, A. Guala, G. Teixid-Tur, L. Galin-Gay, L. Gutirrez, R. Fernndez-Galera, G. Casas, T. Gonzlez-Alujas, I. Ferreira-Gonzlez, A. Evangelista, and J. Rodrguez-Palomares, Diagnostic value of quantitative parameters for myocardial perfusion assessment in patients with suspected coronary artery disease by single- and dual-energy computed tomography myocardial perfusion imaging. *IJC Heart & Vasculature* **32** (2021), 100721.

23. G. Sambuceti, A. L'Abbate, and M. Marzilli, Why should we study the coronary microcirculation? *Amer. J. Physiology-Heart and Circulatory Physiology* **279** (2000), No. 6, H2581–H2584.

24. S. Seitun, C. De Lorenzi, F. Cademartiri, A. Buscaglia, N. Travaglio, M. Balbi, G.P. Bezante, CT myocardial perfusion imaging: A new frontier in cardiac imaging. *BioMed Research International* (2018), 7295460.

25. S. Sen, J. Escaned, I.S. Malik, G.W. Mikhail, R.A. Foale, R. Mila, J. Tarkin, R. Petraco, C. Broyd, R. Jabbou, A. Sethi, C. S. Baker, M. Bellamy, M. Al-Bustami, D. Hackett, M. Khan, D. Lefroy, K. H. Parker, A. D. Hughes, D. P. Francis, C. Di Mario, J. Mayet, and J. E. Davies, Development and validation of a new adenosine-independent index of stenosis severity from coronary wave-intensity analysis: results of the ADVISE (Adenosine Vasodilator Independent Stenosis Evaluation) study. *J. Am. Coll. Cardiol.* **59** (2012), No. 15, 1392–402.

26. S. Simakov, Spatially averaged haemodynamic models for different parts of cardiovascular system. *Russ. J. Numer. Anal. Math. Modelling* **35** (2020), No. 5, 285–294.

27. S. Simakov, T. Gamilov, F. Liang, D. Gognieva, M. Gappoeva, and Ph. Kopylov, Numerical evaluation of the effectiveness of coronary revascularization. *Russ. J. Numer. Anal. Math. Modelling* **36** (2021), No. 5, 303–312.

28. S. Simakov, T. Gamilov, F. Liang, and Ph. Kopylov, Computational analysis of haemodynamic indices in synthetic atherosclerotic coronary netwroks. *Mathematics* **9** (2021), No. 18, 2221.

29. Yu. Vassilevski, V. Yu. Salamatova, and S. S. Simakov, On the elasticity of blood vessels in one-dimensional problems of haemodynamics. *Comput. Math. Math. Phys.* **55** (2015), No. 9, 1567–1578.

30. Yu. V. Vassilevski, A. A. Danilov, T. M. Gamilov, S. S. Simakov, Y. A. Ivanov, and R. A. Pryamonosov, Patient-specific anatomical models in human physiology. *Russ. J. Numer. Anal. Math. Modelling* **30** (2015), No. 3, 185–201.

31. Yu. Vassilevski, M. Olshanskii, S. Simakov, A. Kolobov, and A. Danilov, *Personalized Computational Haemodynamics: Models, Methods, and Applications for Vascular Surgery and Antitumor Therapy*. Academic Press, 2020.

32. M. M. Zaman, S. S. Haque, M. A. Siddique, S. Banerjee, C. M. Ahmed, A. K. Sharma, M. F. Rahman, M. H. Haque, A. I. Joarder, A. U. Sultan, and K. Fatema, Correlation between severity of coronary artery stenosis and perfusion defect assessed by SPECT myocardial perfusion imaging. *Mymensingh Med. J.* **10** (2010), No. 4, 608–613.